Cerebral Cortex September 2015;25:2466–2477
doi:10.1093/cercor/bhu049
Advance Access publication March 20, 2014

Strengthening of Direction Selectivity by Broadly Tuned and Spatiotemporally Slightly Offset Inhibition in Mouse Visual Cortex

Ya-tang Li[1,4], Bao-hua Liu[1], Xiao-lin Chou[1,4], Li I. Zhang[1,3] and Huizhong Whit Tao[1,2]

[1]Zilkha Neurogenetic Institute, [2]Department of Cell and Neurobiology, [3]Department of Physiology and Biophysics, and [4]Graduate Programs, Keck School of Medicine, University of Southern California, Los Angeles, CA 90033, USA

*Address correspondence to Huizhong Whit Tao, Email: htao@usc.edu

Direction selectivity (DS) of neuronal responses is fundamental for motion detection. How the integration of synaptic excitation and inhibition contributes to DS however remains not well-understood. Here, in vivo whole-cell voltage-clamp recordings in mouse primary visual cortex (V1) revealed that layer 4 simple cells received direction-tuned excitatory inputs but barely tuned inhibitory inputs under drifting-bar stimulation. Excitation and inhibition exhibited differential temporal offsets under movements of opposite directions: excitation peaked earlier than inhibition at the preferred direction, and vice versa at the null direction. This could be attributed to a small spatial mismatch between overlapping excitatory and inhibitory receptive fields: the distribution of excitatory input strengths was skewed and the skewness was strongly correlated with the DS of excitatory input, whereas that of inhibitory input strengths was spatially symmetric. Neural modeling revealed that the relatively stronger inhibition under null directional movements, as well as the specific spatial-temporal offsets between excitation and inhibition, allowed inhibition to enhance the DS of output responses by suppressing the null response more effectively than the preferred response. Our data demonstrate that while tuned excitatory input provides the basis for DS in mouse V1, the largely untuned and spatiotemporally offset inhibition contributes importantly to sharpening of DS.

Keywords: direction tuning, excitation/inhibition balance, synaptic input, visual receptive field, voltage-clamp recording

Introduction

The analysis of object motion in the visual world is achieved through actions of direction-selective neurons (Hubel and Wiesel 1962). These neurons respond well to motion in one direction across their visual receptive fields (RFs), but weakly or not at all to motion in the opposite direction. Previous studies in the cat have suggested that direction selectivity (DS) arises anew in the cortex (Wiesel and Hubel 1966; Cleland and Levick 1974; Dreher et al. 1976). Two prominent models have been proposed for the generation of DS. In the first, excitatory response latency shifts systematically across the RF, such that excitatory inputs from different RF locations sum optimally for stimuli moving in the preferred direction (Adelson and Bergen 1985), resulting in direction tuning of excitatory input. This pattern of temporal offsets underlies the well-documented "slant" in spatiotemporal response maps of direction-selective cells (Movshon et al. 1978; Reid et al. 1987, 1991; McLean and Palmer 1989; Albrecht and Geisler 1991; DeAngelis et al. 1993; Emerson 1997; Livingstone 1998). In the second, neither excitation nor inhibition is direction selective, and DS arises from the interplay between excitation and inhibition. In this model, inhibition is spatially asymmetric, i.e., it is preferentially localized to one side of the RF (Barlow and Levick 1965; Torre and Poggio 1978; Hesam Shariati and Freeman 2012). A stimulus moving in the preferred direction evokes a large excitatory response before entering the inhibitory region, whereas a stimulus in the null direction stimulates the inhibitory region first, from which the inhibitory input effectively suppresses the later-activated excitatory input, due to its intrinsically longer delay compared with the excitatory input. More recently, by applying a response latency difference (in milliseconds) to On and Off thalamic relay cells as observed experimentally (Jin et al. 2011), a theoretical study using feedforward networks has successfully modeled cortical DS (Hesam Shariati and Freeman 2012), suggesting that different response latencies for light increments and decrements could also potentially play a role in DS of simple cells that receive relatively balanced On and Off thalamic inputs.

In the cat primary visual cortex (V1), an intracellular study examining excitatory and inhibitory synaptic inputs underlying direction-selective responses of simple cells (Priebe and Ferster 2005) has reported that excitation and inhibition are similarly well tuned for the same direction, which can be attributed to slanted spatiotemporal response maps. In addition, excitation and inhibition are found to be organized in a "push–pull" pattern in the space-time domain, i.e., maximum excitation occurs at the same time as minimum inhibition, and vice versa. Because of the temporal separation between excitation and inhibition, inhibition is not thought to be able to contribute to DS (Priebe and Ferster 2005, 2008). Another study not particularly focusing on simple cells generates a more diverse picture by showing that in a significant portion of V1 cells, maximum inhibition is evoked by null directional stimuli (Monier et al. 2003). In the mouse visual cortex, analysis of the synaptic mechanisms underlying DS has been essentially lacking, despite the emergent importance of this model system for visual research. Recent in vivo Ca^{2+} imaging and single-unit recording studies in the lateral geniculate nucleus (LGN) have suggested that information carried by direction-selective retinal ganglion cells may be channeled into the V1 through direction-selective LGN neurons, which comprise only a small fraction of the mouse LGN population (Rochefort et al. 2011; Marshel et al. 2012; Piscopo et al. 2013; Scholl et al. 2013; Zhao et al. 2013). Consistent with this notion, it is found that thalamocortical input can be direction-tuned (Li, Ibrahim, et al. 2013; Lien and Scanziani 2013), suggesting that direction-tuned LGN input may provide a scaffold for cortical DS in the mouse V1. However, how cortical inhibitory inputs contribute to DS is not known. Recent studies indicate that the "push–pull" relationship between excitation and inhibition as observed in cat simple cells may be absent in the mouse V1 (Liu et al. 2010, 2011; Tan et al. 2011), which suggests that

inhibition can intimately interact with excitation and influence the output response. In this study, we applied in vivo whole-cell voltage-clamp recordings in layer 4 of mouse V1 to reveal excitation and inhibition evoked by moving stimuli. We found in direction-selective cortical neurons that excitation was tuned whereas inhibition was largely untuned. The tuning strength of excitation positively correlated with the spatial skewness of the excitatory input RF, whereas the inhibitory RF was essentially spatially symmetric. The differential spatial tuning between excitation and inhibition was transformed into a temporal asymmetry of excitatory–inhibitory interplay under movements of opposite directions, which facilitated an inhibitory sharpening of DS in the mouse visual cortex.

Materials and Methods

Animal Preparation

All experimental procedures used in this study were approved by the Animal Care and Use Committee of USC. Female adult mice (9–12 weeks, *C57BL/6*) were sedated with an intramuscular injection of chlorprothixene (10 mg/kg in 4 mg/mL water solution) and then anesthetized with urethane (1.2 g/kg, i.p., at 20% w/v in saline). Lactated Ringer's solution was administrated at 3 mL/kg/h to prevent dehydration. The animal's body temperature was maintained at ~37.5°C by a heating pad (Harvard Apparatus). A tracheotomy was performed, and a small glass capillary tube was inserted to maintain a free airway. Cerebrospinal fluid draining was performed. The part of the skull and dura mater (~1 × 1 mm) over the V1 was removed. An artificial cerebrospinal fluid solution (ACSF, containing in millimolar: 140 NaCl, 2.5 KCl, 2.5 $CaCl_2$, 1.3 $MgSO_4$, 1.0 NaH_2PO4, 20 HEPES, 11 glucose, pH 7.4) was applied onto the exposed cortical surface when necessary. The eyes were covered with ophthalmic lubricant ointment until recording, at which time the eyes were rinsed with saline and a thin layer of silicone oil (30 000 centistokes) was applied to prevent drying while allowing clear optical transmission. The eye positions were stable in anesthetized mice, and receptive field drifts were negligible within the recording time windows (Mangini and Pearlman 1980; Niell and Stryker 2008; Liu et al. 2010).

In vivo Electrophysiology

Whole-cell recordings were performed with an Axopatch 200B (Molecular Devices) according to previous studies (Moore and Nelson 1998; Zhang et al. 2003; Liu et al. 2010; Li, Li, et al. 2013). The patch pipette had a tip opening of ~2 μm (4–5 MΩ). With such large pipette openings, our blind whole-cell recordings almost exclusively sampled from excitatory neurons (Liu et al. 2010). For voltage-clamp recordings, the Cs^+-based intrapipette solution contained (in millimolar): 125 Cs-gluconate, 5 TEA-Cl, 4 MgATP, 0.3 GTP, 8 phosphocreatine, 10 HEPES, 10 EGTA, 2 CsCl, 1 QX-314, 0.75 MK-801, pH 7.25. For current-clamp recordings, the K^+-based intrapipette solution contained (in millimolar): 130 K-gluconate, 2 KCl, 1 $CaCl_2$, 4 MgATP, 0.3 GTP, 8 phosphocreatine, 10 HEPES, 11 EGTA, pH 7.25. The pipette capacitance and whole-cell capacitance were compensated completely, and series resistance was compensated by 50%–60% (100μs lag) to achieve 10–15 MΩ effective series resistance. An 11-mV junction potential was corrected. Signals were filtered at 2 kHz for voltage-clamp recording and 5 kHz for current-clamp recording and sampled at 10 kHz. The evoked excitatory and inhibitory currents were separated by clamping cells at −70 and 0 mV, respectively. For cell-attached loose-patch recordings, glass electrodes containing ACSF were used. Instead of a giga-ohm seal, a 100–250-MΩ seal was formed on the targeted neuron. The pipette capacitance was completely compensated. The spike signal was filtered at 10 kHz and sampled at 20 kHz. In order to record from fast-spiking (FS) inhibitory neurons, smaller pipettes (10 MΩ) were used and neurons with fast-spike shapes were actively searched. One FS neuron could be encountered for every 5–10 attempts. All neurons recorded in this study were located at a depth of 375–500 μm below the pia according to the microdrive reading, corresponding to layer 4 (Li, Ma, Li, et al. 2012).

Visual Stimulation

Stimuli were created using Matlab with Psychophysics Toolbox and displayed with a gamma-corrected LCD monitor (refresh rate 75 Hz) placed 0.25 m away from the right eye. The center of the monitor was placed at 45° azimuth, 25° elevation, and it covered ±35° horizontally and ±27° vertically of the mouse visual field. Recordings were made in the monocular zone of the V1. Spontaneous activity was recorded when a uniform gray background (luminance: 41.1 cd/m^2) was applied. The On/Off receptive field of the cell was first roughly mapped with a set (6 × 8) of flash bright (57.5 cd/m^2) and dark (24.7 cd/m^2) squares (10° size) in pseudorandom sequence to determine the preferred contrast. Drifting sinusoidal gratings (2 Hz, 0.04 cycle/degree, 95% contrast) at 12 directions (30° step) were applied to measure the response modulation as to determine the simple/complex cell type. For this type of stimulation, stationary grating of one orientation was first presented on the full screen for 1.8 s before it drifted for 1.5 s. The grating stopped drifting for 500 ms before another grating pattern appeared. The twelve patterns were presented in a random sequence and were repeated for 5–10 times. To examine synaptic inputs underlying DS, drifting bars (4° width, 60° length, 50°/s speed, 95% contrast, light or dark) of 12 directions were applied for 5–10 repetitions. Drifting bars were used because they are a simple type of stimulation and mainly test responses to a single polarity of contrast. In addition, it is easier to correlate the properties of moving-bar-evoked responses with the spatial-temporal patterns of underlying inputs compared with moving-grating-evoked responses. Bars moved across the screen with an inter-stimulus interval of 1.5 s. For cells tested with both drifting gratings and drifting bars, the same preferred direction was revealed ($n = 12$, data not shown). To map spatial RFs, bars (4° width, 60° length) of optimal orientation and contrast at 15 positions were flashed (duration = 80 or 120 ms, inter-stimulus interval = 500 ms) in a pseudorandom sequence (i.e., sequence was designed to avoid stimulating adjacent RF locations sequentially). Each location was stimulated 10 times. Using 80- and 120-ms flashing bars generated similar spatial tuning curves (data not shown).

Data Analysis

Spikes were sorted offline. Spike shape was determined by averaging 50–100 individual spikes. Fast-spiking neurons were identified by a narrow spike shape (tough-to-peak interval <0.5 ms). Spikes evoked by drifting gratings were counted within a 70–2570-ms window after the start of drifting. The mean spontaneous firing rate in the absence of visual stimulation was subtracted from the stimulus-evoked spike rates. Spike responses for each grating stimulus were cycled-averaged across trials. The sinusoidal fitting of cycle-average responses at preferred direction was used to calculate the mean (F0) and modulation amplitude (F1). Those neurons with modulation ratios (F1/F0) larger than 1 were considered simple cells. Monocontrast index was calculated as the difference between peak response levels in On and Off subfields (On–Off), divided by their sum. The index is 1 if the cell only shows spike responses to On contrast and −1 if the cell only shows responses to Off contrast. In current-clamp recordings with the K^+ gluconate-based intrapipette solution, spikes were removed with an 8-ms median filter (Li, Ma, Li, et al. 2012) and the residual subthreshold V_m response was analyzed. In voltage-clamp recordings, the excitatory and inhibitory response traces were first smoothed by averaging within a sliding 40-ms window (Li, Ma, Li, et al. 2012), and the peak response relative to the baseline was then determined and used to plot tuning curves. The peak intracellular or spike responses across directions were fit with 2 Gaussian curves centered on φ_{pref} and $\varphi_{pref} + 180$, of equal variances (σ^2) but different amplitudes (A_1 and A_2):

$$R(\varphi) = A_1 \times \exp\left[\frac{-0.5 \times (\varphi - \varphi_{pref})^2}{\sigma^2}\right] + A_2 \times \exp\left[\frac{-0.5 \times (\varphi - \varphi_{pref} - \pi)^2}{\sigma^2}\right] + B$$

Direction preference was calculated based on the vector sum of the peak responses across directions. ANOVA test was performed to determine whether at least response at one direction was significantly above

others. Gaussian fitting was performed for cells that passed this test. From this fit, we calculated a direction-selectivity index as DSI = $(R_{pref} - R_{null})/(R_{pref} + R_{null})$, where $R_{pref} = A_1 + B$ and $R_{null} = A_2 + B$. The RF envelope of peak excitatory and inhibitory synaptic amplitudes was fitted with a skew-normal distribution function:

$$f(x) = \text{amplitude} \times \frac{2}{\omega}\varphi\left(\frac{x-\xi}{\omega}\right) \times \Phi\left(\alpha\left(\frac{x-\xi}{\omega}\right)\right) + \text{baseline}$$

where φ and Φ are the standard normal probability density function and its cumulative distribution function, respectively, ξ determines the location, ω is the scale factor, and α is the shape factor. The skewness is given by the following:

$$\text{skewness} = \frac{4-\pi}{2}\frac{\left(\delta\sqrt{\frac{2}{\pi}}\right)^3}{\left(\frac{1-2\delta^2}{\pi}\right)^{3/2}}, \quad \text{with } \delta = \frac{\alpha}{\sqrt{1+\alpha^2}}$$

Positive skewness indicates that the tail of the spatial tuning curve on the null side of the cell is longer than the preferred side. Conversely, negative skewness indicates that the tail on the preferred side is longer than the null side.

The temporal overlap between excitatory and inhibitory response traces, and the spatial overlap between excitatory and inhibitory RFs was quantified with an overlap index (OI), which is given by: OI = $(w_1 + w_2 - d)/(w_1 + w_2 + d)$, where w_1 and w_2 are the half-widths at half-maximum of excitatory and inhibitory response waveforms or tuning curves, respectively, and d is the distance between the peaks of the 2 response waveforms or tuning curves under comparison. OI = 1 gives a complete overlap, and OI $\leq$ 0 gives a complete separation.

Neuron Model

Excitatory and inhibitory conduces were derived as previously described (Liu et al. 2010; Zhang et al. 2011; Li, Ma, Pan, et al. 2012), according to the following equation:

$$I(t) = G_r(V_m(t) - E_r) + G_e(t) \times (V_m(t) - E_e) + G_i(t) \times (V_m(t) - E_i)$$

where $I(t)$ is the amplitude of current at a time point; G_e and G_i are the excitatory and inhibitory synaptic conductance, respectively; G_r is the resting conductance and was determined based on the baseline currents at different potentials; $V_m(t)$ is the membrane voltage at time t; E_e (0 mV) and E_i (−70 mV) are the reversal potentials; E_r is the resting membrane potential; $V_m(t)$ is corrected by $V_m(t) = V_h - R_s \times I(t)$, where R_s was the effective series resistance and V_h is the applied holding voltage.

We derived the membrane potential response in the absence of a spiking mechanism by feeding the experimentally determined excitatory and inhibitory conductances into an integration-fire neuron model, which is basically a leaky-RC circuit without the spiking mechanism:

$$V_m(t + dt) = -\frac{dt}{C}[G_e(t) \times (V_m(t) - E_e) + G_i(t) \times V_m(t) - E_i) + G_r(V_m(t) - E_r)] + V_m(t)$$

where $V_m(t)$ is the membrane potential at time t, and C is the whole-cell capacitance. C was measured during the experiment and G_r was calculated based on the equation $G_r = C \times G_m/C_m$, where G_m, the specific membrane conductance, is 2e–5 S/cm^2, and C_m, the specific membrane capacitance, is 1e–6 F/cm^2.

Simulation

We simulated the moving-bar response as the sum of responses to 15 sequential bars (4° width) evenly spaced in time, corresponding to a moving speed of 50°/s. All the individual bar responses had the same temporal profile. They were modeled as follows:

$$G = G_{max} \times \left(1 - \exp\left(\frac{-(t-t_0)}{\tau_1}\right)\right) \times \exp\left(\frac{-(t-t_0)}{\tau_2}\right), \quad \text{for } t > t_0$$

where t_0 is the response onset latency. Fitting of the average response to flash bars yielded $\tau_1 = 2.8$ s and $\tau_2 = 0.04$ s. For each bar, G_{max} was determined by its location within the RF. The RF spatial tuning curve was modeled as a skew-normal distribution function. The latency t_0 was negatively linearly correlated with the response amplitude, with the shortest latency = 50 ms and longest latency = 100 ms.

Results

Direction Selectivity of Layer 4 Neurons in Mouse V1

With in vivo cell-attached loose-patch recordings (Wu et al. 2008; Zhou et al. 2010), we first examined DS properties of layer 4 neurons in the mouse V1. These neurons have been shown to receive direct thalamocortical input (Li, Ibrahim, et al. 2013; Lien and Scanziani 2013). The recorded cells were categorized into putative excitatory and FS inhibitory neurons, according to their spike widths (Fig. 1*A*). Direction tuning was assayed by applying single drifting bars or drifting gratings at twelve evenly spaced directions (see Materials and Methods). We quantified the strength of tuning with a DSI. DSI > 0.3 was used as a criterion for defining direction-selective neurons (note that 0.2 was used in [Conway and Livingstone 2003]). In our recorded excitatory neurons, about half (28 out of 52) were direction-selective (Fig. 1*B*). In contrast, the FS neurons, which were putative parvalbumin-positive inhibitory neurons (Liu et al. 2009; Ma et al. 2010), exhibited much weaker DS (Fig. 1*B*). They were essentially untuned for direction (DSI < 0.3), consistent with several previous reports (Niell and Stryker 2008; Ma et al. 2010).

Layer 4 excitatory neurons exhibited linear responses to drifting sinusoidal gratings, as demonstrated by F1/F0 ratios larger than 1 (Fig. 1*C*), which are a prominent feature of simple cells (Skottun et al. 1991). Notably, the receptive fields (RFs) of these neurons were largely dominated by responses to one polarity of stimulus contrasts (On or Off), as demonstrated by monocontrast indices close to 1 or −1 (Fig. 1*D*). In contrast, neurons in superficial layers (layer 2/3) exhibited more or less similar responsiveness to light increments (On) and decrements (Off) (Fig. 1*D*). Considering these response properties, the layer 4 excitatory neurons mostly resembled previously described "S1" neurons in the cat/primate (Schiller et al. 1976; Conway and Livingstone 2003), i.e., simple cells with only 1 receptive field subregion. Possibly due to this monocontrast property, the direction-selective layer 4 neurons exhibited the same preferred direction when tested with light and dark drifting bars (Fig. 1*E*). This could be explained by the observation that the response to a bar of non-optimal contrast in fact reflected the "Off" discharge when the bar left the subfield of the dominating contrast, as demonstrated by the increasing delay of the "Off" discharge with increasing bar widths (Fig. 1*F*). Since light and dark bars generated responses showing the same preferred direction, in the next experiments, we applied drifting bars of the contrast the cell was most sensitive to.

Direction Tuning of Subthreshold Response

By applying whole-cell current-clamp recording with a K^+ gluconate-based internal solution (see Materials and Methods), we compared DS of spike and membrane potential (Vm) responses of the same neuron. Figure 2*A* shows the peristimulus spike time histograms (PSTHs) for spike responses of a layer 4 excitatory neuron to drifting bars at 12 different directions, as well as its subthreshold Vm responses after filtering out spikes (see Materials and Methods). The cell responded

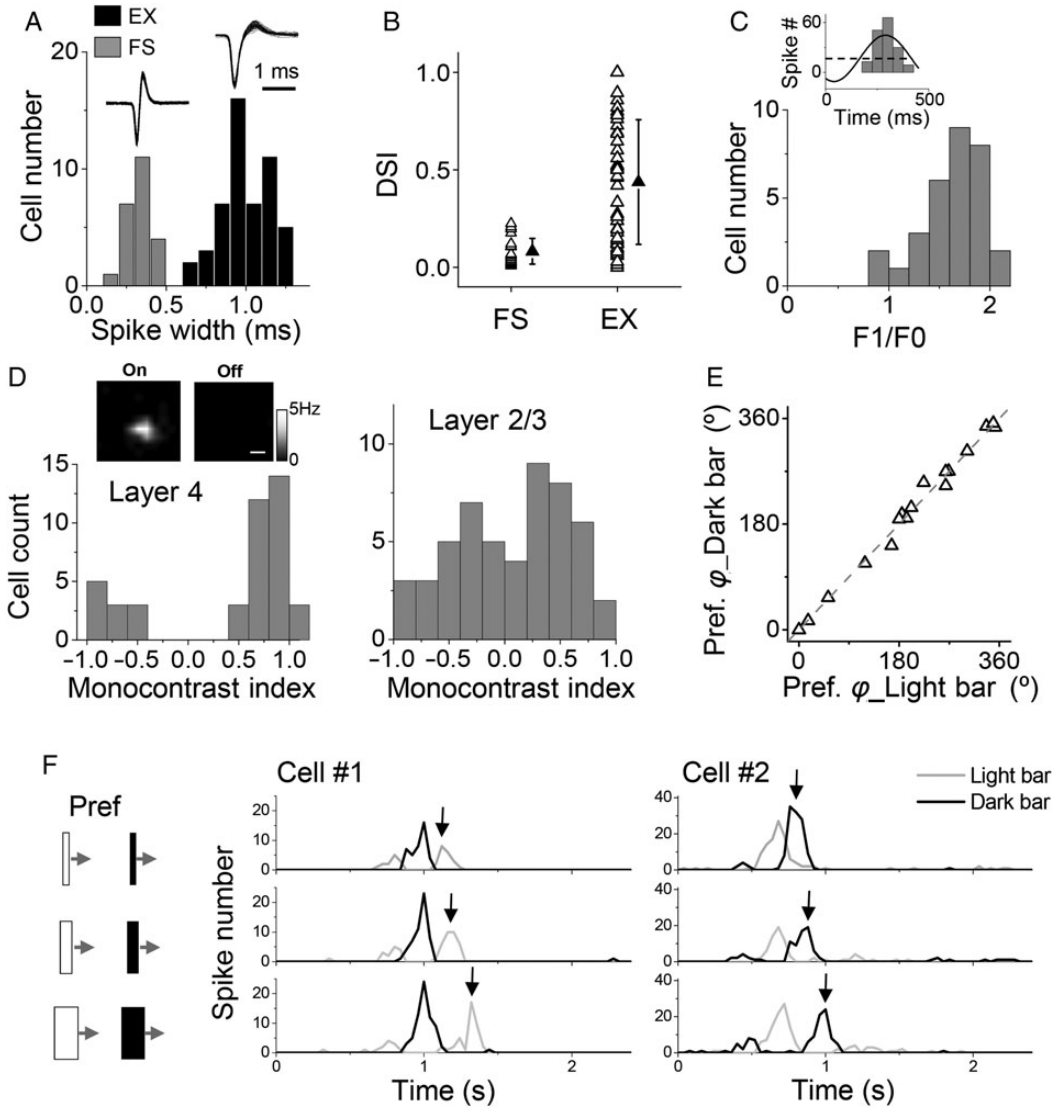

Figure 1. Direction selectivity of layer 4 neurons in mouse V1. (*A*) Distribution of spike widths for all recorded layer 4 neurons. Spike width was quantified as the interval between the trough and peak of the average spike waveform of the cell. Fast-spiking cells had spike widths of <0.5 ms. EX, putative excitatory cells. Superimposed 50 individual spikes are shown for an example FS and EX cell, respectively (top inset). (*B*) DSIs of recorded FS ($n = 23$) and excitatory ($n = 52$) neurons. Solid symbols represent mean ± SD. (*C*) Distribution of F1/F0 ratios for layer 4 excitatory neurons. Top inset, cycle-averaged PSTH for spike responses (baseline subtracted) of an example cell to drifting sinusoidal gratings at the preferred direction, fit to a sinusoid (black line). Black dash line indicates F0. (*D*) Distribution of monocontrast indices for excitatory neurons in layer 4 (left) and layer 2/3 (right). The index is 1 or −1 if the cell only shows spike responses to one contrast (On or Off, respectively). Top inset, spatial maps of On and Off spike responses of an example layer 4 cells, which showed only an On subfield. Scale bar: 10°. (*E*) The preferred directional angle φ measured with dark drifting bars versus that measured with light drifting bars. Gray dash line is the identity line. Each data point represents 1 cell. (*F*) PSTH for spike responses of 2 representative cells to bright and dark drifting bars of preferred orientation and different bar widths (4°, 8°, 16°, illustrated on the left). Cell#1 had a dominant "Off" subfield. Black arrows mark the discharge response to the withdrawal of the light bar from the Off subfield, the timing of which changed with increasing bar width. Cell#2 had a dominant "On" subfield.

maximally to a vertical bar drifting to the right, while having little response to a bar drifting to the left, indicating that it was strongly direction selective. Different from the spike responses, robust membrane depolarization responses were observed at all directions. The polar graph plots of spike count and peak depolarization voltage demonstrate that the strongest spike and Vm responses occurred at the same direction (Fig. 2*A*, bottom panel). The spike response exhibited much stronger selectivity than the Vm response, as reflected by the relative difference between the response magnitudes to the preferred and opposite (null) directions.

We recorded from a total of 25 layer 4 excitatory neurons and calculated DSIs after fitting their response tuning curves with a wrapped Gaussian function (see Materials and Methods). As shown in Figure 2*B*, DSI of spike response positively correlated with that of Vm response, but its value was much higher than that of the Vm response. Notably, DS had been amplified ~6-fold when Vm response was transformed into spike response. This result is in agreement with the notion that spike thresholding can be a powerful mechanism for sharpening feature selectivity of neuronal responses (Priebe and Ferster 2008). In all the recorded neurons, strongest spike and Vm responses were observed at identical or nearly identical directions (Fig. 2*C*). According to these results, direction-selective neurons can be predicted based on the DSI of their Vm responses. In this study, we set this value at >0.05 (corresponding to spike DSI > 0.3) as a criterion for identifying putative direction-selective neurons.

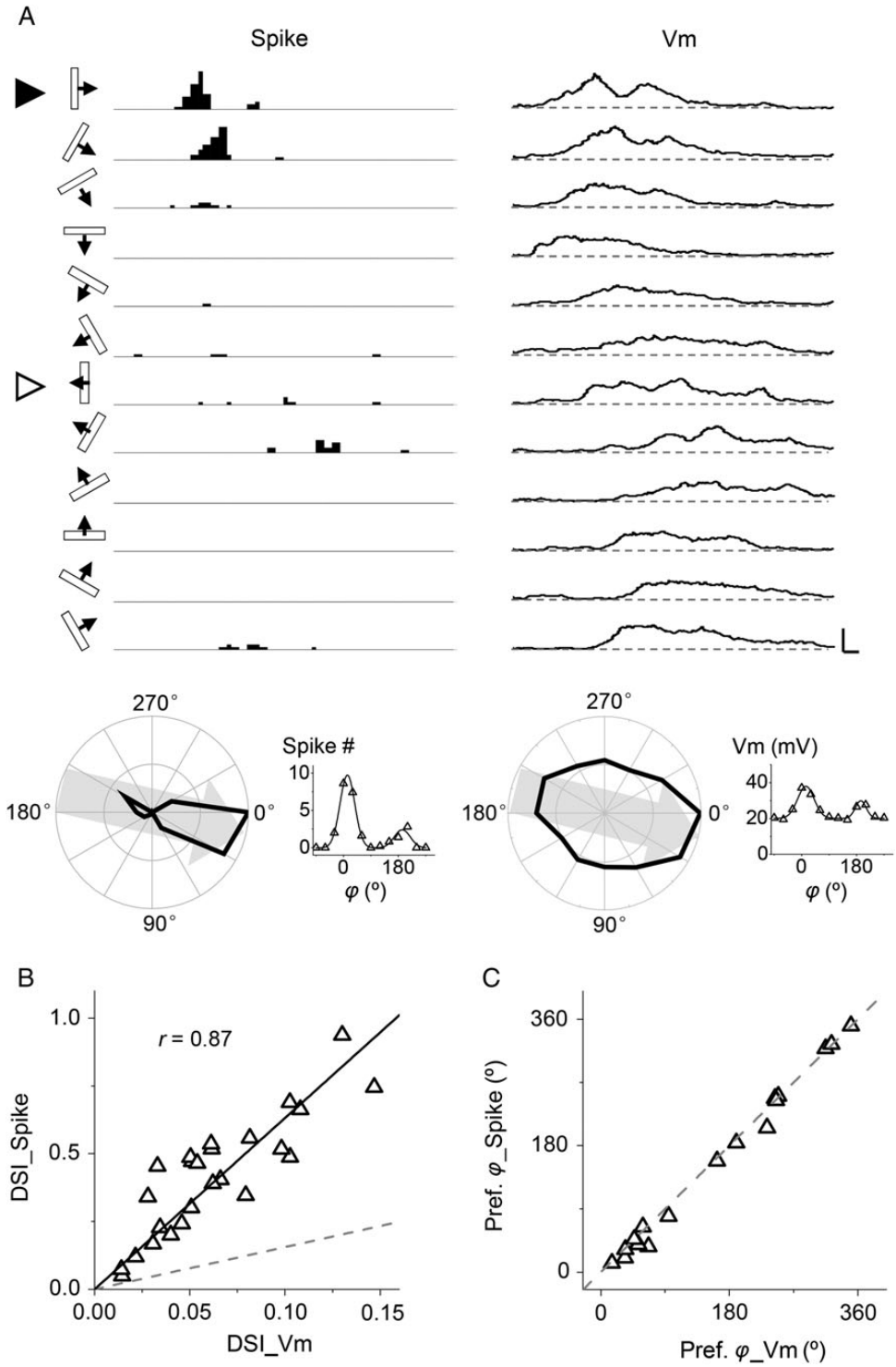

Figure 2. Direction tuning of subthreshold membrane potential (Vm) response. (*A*) Current-clamp recording from an example cell. Left, PSTHs for spike responses to drifting bars at 12 directions. Right, average Vm responses (10 trials) after filtering out spikes. Scale: 40 Hz/18 mV, 100 ms. The stimulus direction is indicated on the left. Solid arrowhead marks the preferred direction and open arrowhead marks the null direction. Bottom panel, polar graph (left) and tuning curve (right) of spike count and peak Vm responses. Gray arrow indicates the preferred direction. Gaussian fits are shown. (*B*) DSI of peak spike rate versus that of peak Vm response. Gray dash line is the identity line. Black solid line is the best-fit linear regression line. The correlation coefficient *r* is indicated. (*C*) The preferred direction of spike response versus that of Vm response for cells with DSI > 0.2. Gray dash line is the identity line.

Direction Tuning of Excitatory and Inhibitory Synaptic Inputs

To address excitatory and inhibitory interactions underlying DS, we applied in vivo whole-cell voltage-clamp recording with a Cs^+-based internal solution to isolate excitatory and inhibitory synaptic currents evoked by drifting bars (see Materials and Methods). Neurons were first recorded under current-clamp mode to determine the tuning of their Vm

responses. Excitatory currents were then recorded by clamping the cell's membrane voltage at −70 mV, and inhibitory currents were recorded at 0 mV (Liu et al. 2010, 2011). As shown by an example cell in Figure 3*A*, we first determined that the cell was likely a direction-selective cell, as its Vm response had a DSI of 0.14. Its excitatory responses displayed a clear direction bias, which was the same as that of the Vm response. A direction bias of its inhibitory responses however was not obvious, indicating that the inhibition was nearly untuned.

In a total of 19 putative direction-selective excitatory cells, we observed that the preferred direction of Vm responses was essentially identical to that of excitatory inputs (Fig. 3*B*). More importantly, the DSI value for Vm responses strongly correlated with that for excitatory inputs (Fig. 3*C*). These results support the notion that DS of layer 4 excitatory neurons originates from direction-tuned excitatory input. That is, the initial bias of excitatory input sets the basis for DS. In a total of 12 cells with Vm DSI > 0.05 and with both excitatory and inhibitory responses recorded, we found that DSI of inhibition was always lower than that of excitation (Fig. 3*D*). The average DSI for inhibition was 0.04 ± 0.01 (mean ± SD, $n = 12$), whereas that for excitation was 0.12 ± 0.02 ($P < 0.001$, paired *t*-test). Nevertheless, the preferred direction of inhibition was essentially the same as that of excitation (Fig. 3*E*). Therefore, the strongest inhibition was evoked by a bar that also evoked the strongest excitation, but the direction tuning of inhibition was much weaker than that of excitation. The largely untuned property of synaptic inhibition was consistent with the observation that FS inhibitory neurons were mostly untuned (Fig. 1*B*).

Inhibition Sharpens Direction Selectivity of Output Responses

Due to the differential tuning of excitation and inhibition, i.e., inhibition being much less selective than excitation, the excitation/inhibition (E/I) ratio was significantly lower at the null than the preferred direction (Fig. 4*A*). This differential E/I balance for preferred and null directional stimuli may potentially lead to a sharpening of DS of output responses. To test this possibility, we compared the temporal profiles of excitatory and inhibitory responses to the same drifting bar. Different from previous results in the cat V1 (Priebe and Ferster 2005), we found that for both preferred and null directions, there was a large temporal overlap between excitation and inhibition (Fig. 4*B*). The average temporal OI between excitatory and inhibitory response traces (see Materials and Methods) was 0.78 ± 0.07 (mean ± SD) for the preferred direction, and 0.83 ± 0.10 for the null direction. This indicates that inhibition can closely interact with excitation and suppress the membrane depolarization response at both the preferred and null directions and that inhibition may exert a sharpening effect by suppressing the null response more effectively than the preferred response.

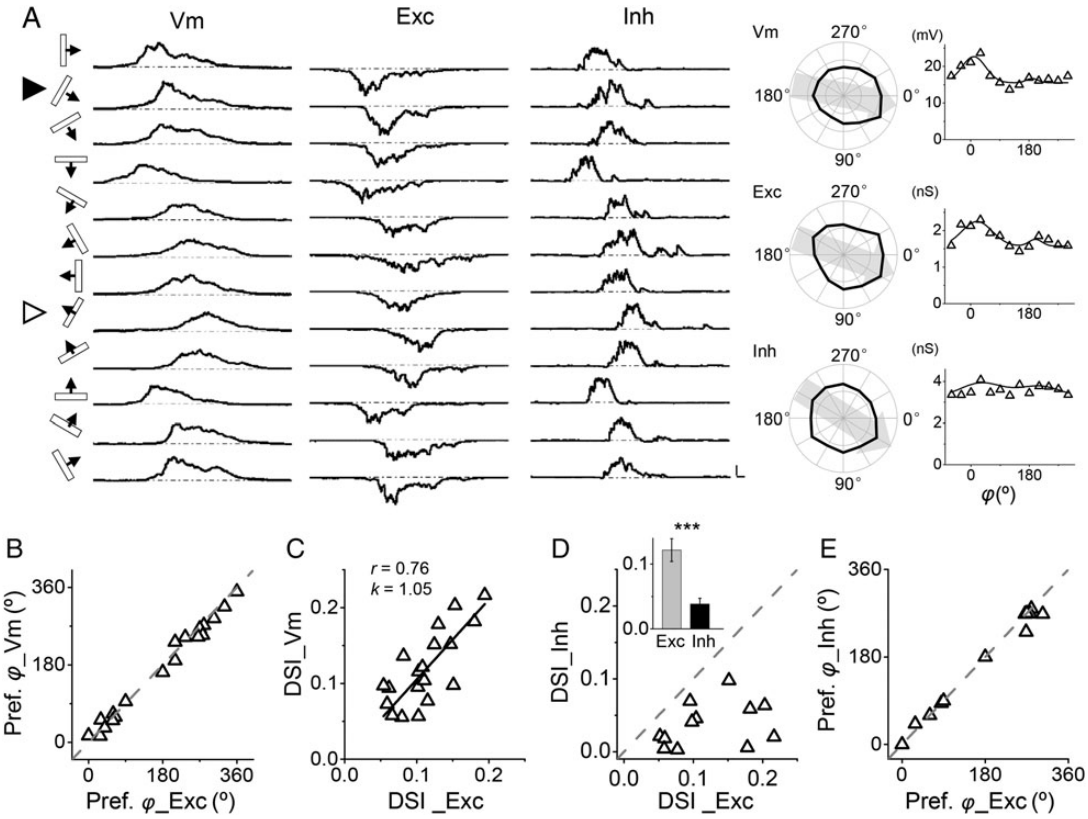

Figure 3. Direction tuning of excitatory and inhibitory synaptic inputs. (*A*) Left panel, sequentially recorded Vm, excitatory (Exc), and inhibitory (Inh) responses to drifting bars in an example cell. Scale, 10 mV/68 pA/121 pA, 100 ms. Right panel, corresponding polar graphs and tuning curves. Solid arrowhead indicates the preferred direction. (*B*) The preferred directional angle of Vm response versus that of excitatory input ($n = 20$). Gray dash line is the identity line. (*C*) DSI of Vm response versus that of excitatory input. Black solid line is the best-fit linear regression line. The correlation coefficient *r* and slope *k* are indicated. (*D*) DSI of inhibition versus that of excitation. Gray dash line is the identity line. In this analysis, only cells with DSI_Vm > 0.05 were included. Inset, average DSI of excitation (gray) and inhibition (black). ***$P < 0.001$, paired *t*-test, $n = 12$. (*E*) The preferred directional angle of inhibition versus that of excitation. Gray dash line is the identity line.

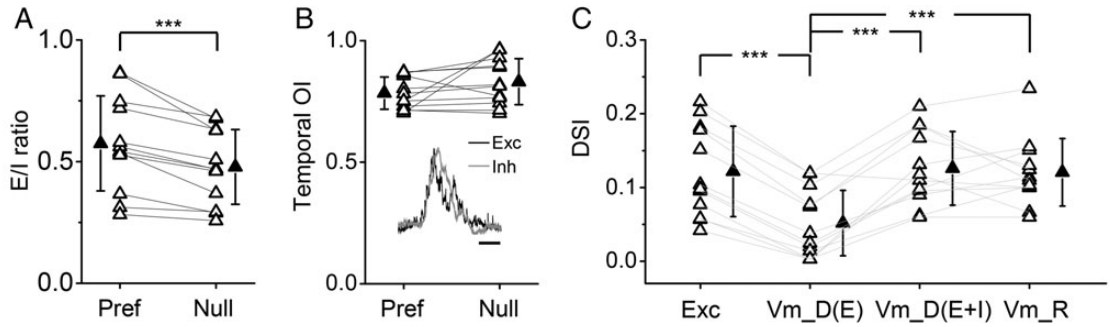

Figure 4. Inhibition sharpens DS of membrane potential response. (*A*) E/I ratios for responses at preferred and null directions. Data points for the same cell are connected with a line. ***P = 1.7e-4, one-tailed paired t-test, n = 12. Solid symbols represent mean ± SD. (*B*) Temporal overlap indices for excitatory and inhibitory responses at preferred and null directions (P = 0.12, two-tailed paired t-test, n = 12). Inset, superimposed normalized excitatory and inhibitory conductances evoked by the same moving bar in an example cell. Scale: 0.5 s. (*C*) DSI of excitatory input (Exc), derived Vm response when only excitation is present (Vm_D(E)), derived Vm response when both excitation and inhibition are present (Vm_D(E + I)) and of recorded membrane potential response (Vm_R). ***P < 0.001, one-way ANOVA and post hoc test, n = 12. Data from the same cell were connected. DSI of Exc is not significantly different from that of Vm_D(E + I) or Vm_R.

To directly test the inhibitory influence on DS, we applied a conductance-based integrate-and-fire neuron model (Liu et al. 2010, 2011; Li, Ma, Li, et al. 2012) to derive the expected membrane potential (Vm) responses in the presence and absence of inhibition. The experimentally determined excitatory and inhibitory conductances evoked by drifting bars were applied in the neuron model (see Materials and Methods). As shown in Figure 4*C*, when excitatory inputs (Exc) alone were transformed into Vm responses (Vm_D(E)), there was a significant reduction in the strength of selectivity. This observation is consistent with previous reports that the nonlinear membrane filtering attenuates response selectivity (Liu et al. 2011). To be more specific, because the relationship between the Vm response amplitude and excitatory conductance (i.e., input-output function) is a concave and saturating function (Liu et al. 2011), the Vm response amplitude relative to the excitatory conductance is smaller at larger excitatory conductances. This could be partly due to the fact that the driving force for excitatory currents is reduced as larger excitatory postsynaptic potentials (EPSPs) are generated (Liu et al. 2011). As the excitatory inputs were only moderately tuned, the attenuation of selectivity would result in largely untuned Vm responses. Noticeably, when inhibition was incorporated, the selectivity of Vm responses (Vm_D(E + I)) was markedly enhanced (Fig. 4*C*). More importantly, DSI of derived Vm responses became similar to that of experimentally observed Vm responses (Vm_R). These modeling results demonstrate that inhibitory inputs indeed have sharpened DS of output responses.

Temporal Offset Between Peak Excitation and Inhibition

Are there any other factors contributing to the inhibitory effect on DS besides the different E/I ratio for opposite moving directions? When comparing the excitatory and inhibitory response traces evoked by the same drifting bar stimulus, we found that although excitation and inhibition were largely overlapping in the temporal domain, their peak response time was different (Fig. 5*A*). Excitation peaked earlier than inhibition at the preferred direction, whereas this temporal sequence was reversed at the null direction (Figs 5*A*,*C*). In addition, the excitatory responses themselves exhibited a temporal asymmetry: the interval between the response onset and response peak was shorter at the preferred than the null direction (Fig. 5*D*). On the other hand, such temporal asymmetry was not observed for inhibitory responses: the peak time relative to the onset was about the same for the preferred and null directions (Fig. 5*E*). Since excitation rises to the maximum faster than inhibition for movements in the preferred direction but slower than inhibition for movements in the null direction, inhibition could be more effective in suppressing the excitatory response to the null direction, thus contributing to the sharpening of DS of output responses.

Spatially Asymmetric Excitatory and Symmetric Inhibitory Receptive Fields

The above temporal properties of synaptic responses suggest that the spatial organization of the excitatory input RF may be asymmetric so that it takes a bar a shorter time to arrive at the RF peak when it comes from the preferred side than from the null side. To test this possibility, we mapped the spatial RFs of synaptic responses with flashing bars of optimal orientation and contrast at different spatial locations (see Materials and Methods). First of all, we found that consistent with the temporal overlap between excitation and inhibition evoked by moving stimuli, the excitatory and inhibitory RFs almost completely overlapped in the spatial domain (Fig. 5*B*). The average spatial OI was 0.78 ± 0.08 (n = 12, Fig. 5*F*). Second, as shown by the average response traces of 2 example cells, the spatial distribution of peak amplitudes of flash-bar-evoked excitatory responses was skewed toward the preferred side, manifested by a longer tail of the spatial tuning curve on the right than the left side (Fig. 5*B*, the red curve). A summary of 16 cells showed a strong positive correlation between skewness of the excitatory RF and DSI of moving-bar-evoked excitatory responses (Fig. 5*G*). In addition, the excitatory RF was always skewed toward the side consistent with the cell's preferred direction, as manifested by positive skewness values (Fig. 5*G*). Together the results indicate that the stronger the RF skewness the more selective are the moving-bar-evoked excitatory responses. Third, the inhibitory RF was much more spatially symmetric compared with the excitatory RF in the same cell, as shown by the close-to-zero skewness value (Fig. 5*H*). This result is also consistent with the observation that inhibitory responses to preferred and null directional movements had a similar peak time (Fig. 5*E*). Due to the differential spatial asymmetry of excitatory and inhibitory RFs, the inhibitory RF peak was displaced toward the null side of the cell relative to its excitatory counterpart (Figs 5*B*,*I*). This spatial offset between excitatory

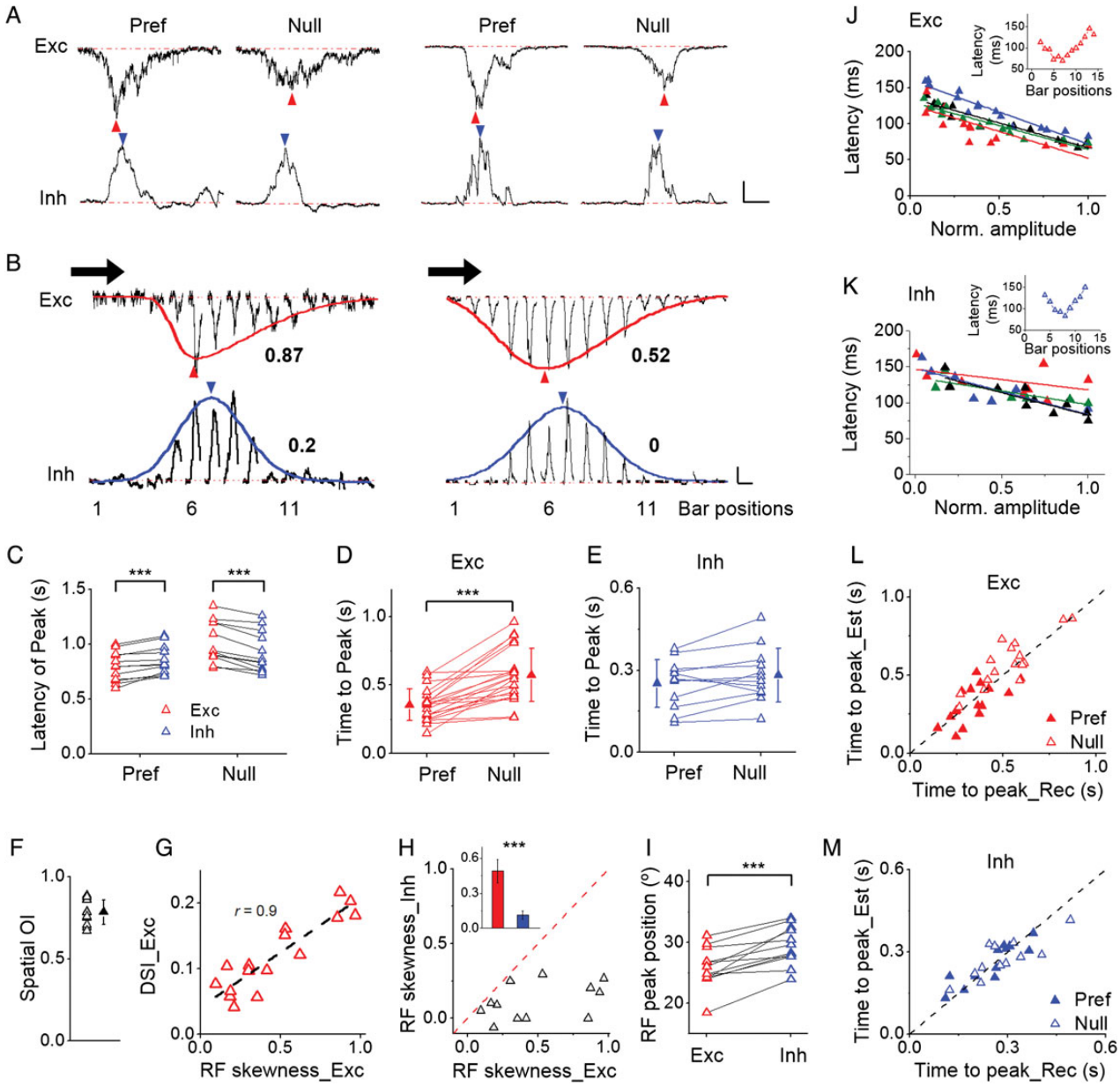

Figure 5. Temporal and spatial offsets between excitation and inhibition. (*A*) Excitatory and inhibitory responses to preferred and null directions in 2 example cells. Scale: 20/58 pA (Exc); 46/104 pA (Inh), 450 ms. Blue and red arrowheads mark peak response times. (*B*) Excitatory and inhibitory RFs mapped with flashing bars in the same cells as shown in (*A*). Response traces were aligned according to the corresponding bar positions. The preferred direction of the cell is marked by the black arrow. Red and blue curves represent skew-normal fitting of the RFs. Arrowheads mark their respective peaks. The skewness values are indicated. Scale: 10/21 pA (Exc); 20/40 pA (Inh), 450 ms. (*C*) Latencies of peak excitation (red) and peak inhibition (blue) relative to the response onset at preferred ($P = 1.8e\text{-}4$, paired *t*-test, $n = 12$) and null ($P = 1.2e\text{-}5$, paired *t*-test, $n = 12$) directions. (*D*) Time intervals from response onset to response peak for excitatory responses at preferred and null directions ($P = 2.7e\text{-}6$, paired *t*-test, $n = 21$). Data from the same cell are connected. (*E*) Time intervals from response onset to response peak for inhibitory responses ($P = 0.064$, two-tailed paired *t*-test, $n = 12$). (*F*) Spatial overlap indices between spatial tuning of excitatory and inhibitory responses. Solid symbols represent mean ± SD. (*G*) DSI of excitatory input versus skewness of excitatory RF ($n = 16$). Dash line is the best-fit linear regression lines. The correlation coefficient *r* is indicated. Note that all skewness values are positive, indicating that all the excitatory RFs are skewed toward the preferred side of the cell. (*H*) Skewness of inhibitory RF versus that of excitatory RF. Inset, average skewness (red for excitation, blue for inhibition, $P = 6e\text{-}4$, paired *t*-test, $n = 12$). Bar = SEM. (*I*) Location of RF peak relative to the preferred side of the cell for excitation and inhibition ($P = 1.8e\text{-}4$, paired *t*-test, $n = 12$). (*J*) Onset latency of each flashing-bar-evoked excitatory response versus its peak amplitude (normalized to the maximum value in the same cell). Each color represents 1 cell. The best-fit linear regression lines are shown. Inset, onset latencies of excitatory responses evoked by flashing bars at different positions in an example cell. (*K*) Onset latency of each flashing-bar-evoked inhibitory response versus its relative peak amplitude. (*L*) Plot of estimated time for a bar to move from the RF boundary to the RF peak against the observed time interval between the onset and peak of excitatory responses to preferred (solid) and null (open) directional movements. Dash line is the identity line. (*M*) Plot in the same way as (*L*) for inhibitory responses.

and inhibitory RF peaks ($3.8 \pm 2.3°$, $n = 12$) was small compared with the overall RF sizes ($40.6 \pm 10.3°$, $n = 12$) but was highly significant ($P < 0.001$, paired *t*-test).

The temporal offset between peak excitation and inhibition evoked by a moving stimulus (Fig. 5*C*) is consistent with the spatial offset between peak excitation and inhibition evoked by stationary (flash) stimuli, suggesting that the spatial relationship has been translated into a matching temporal relationship. To further demonstrate this point, we predicted the timing of peak excitation/inhibition under moving stimuli

based on the spatial RF property. We first analyzed the onset latency of each flashing-bar-evoked synaptic response. We found that in general the latency correlated negatively with the peak response amplitude (Figs 5*J*,*K*), so that the latency at the RF peak (where the strongest response was evoked) was shorter than that at RF peripheries (Figs 5*J*,*K*, inset). Taking the onset latencies of flashing-bar responses and the moving bar speed into consideration, the predicted timing of peak synaptic response generally matched the experimentally observed value (Figs 5*L*,*M*), indicating that the timing of peak moving-bar-evoked response reflected the timing when the RF peak was stimulated.

The Spatial Offset between Excitation and Inhibition Contributes to DS

To better understand how the RF organization might contribute to DS, we performed simulations with a conductance-based neuron model (Zhang et al. 2003). The moving-bar-evoked response was simulated as a sum of responses to sequential flashing bars evenly spaced in time (see Materials and Methods). For simplicity, the modeled flashing-bar responses had similar temporal profiles except that their onset delays depended on their response amplitudes in a linear fashion (Fig. 6*A*). The latter then depended on bar locations within the RF. To be consistent with our experimental observation that the average onset latency difference between flash-stimulus-evoked excitation and inhibition was 18 ms (Fig. 6*B*), in our model each flashing-bar-evoked inhibitory response was delayed relative to the excitatory response by 18 ms ($\Delta T = 18$ ms). After summing up the individual-bar-evoked responses (Fig. 6*C*, upper panel), the resulting moving-bar-evoked excitatory and inhibitory conductances were fed into the neuron model to derive the expected Vm response (Fig. 6*C*, lower panel). DSI was calculated from the peak Vm responses to preferred and null directions.

The modeled excitatory and inhibitory RFs completely overlapped (Fig. 6*D*, inset). We varied the skewness of the excitatory RF while keeping the inhibitory RF symmetric (Fig. 6*D*, inset). This generated a varying spatial offset between excitatory and inhibitory RF peaks (ΔX_peak). When both the excitatory and inhibitory RFs were symmetric (i.e., ΔX_peak = 0), the Vm response was not direction-tuned (DSI_Vm = 0) (Fig. 6*D*, black). As the excitatory RF became skewed and ΔX_peak increased, DSI of Vm responses quickly increased and then declined (Fig. 6*D*, black), suggesting that a small spatial offset is sufficient and optimal for producing tuned output responses. The positive value of DSI indicates that the preferred side is exactly the side toward which the excitatory RF is skewed, which is consistent with our experimental observation (Fig. 5*G*). Therefore, a skewed excitatory RF plus non-skewed inhibitory RF can lead to correct directionality of output responses. The RF skewness *per se* however does not directly result in direction-tuned synaptic responses, as the simulated moving-bar-evoked excitatory response was not direction-tuned (Fig. 6*E*, red). In addition, when excitatory and inhibitory RFs were both skewed but without a spatial offset (ΔX_peak = 0), no direction-tuned output response was generated (Fig. 6*E*, black). Therefore, the effect shown in Figure 6*D* could only be attributed to a result of the spatial offset between excitation and inhibition.

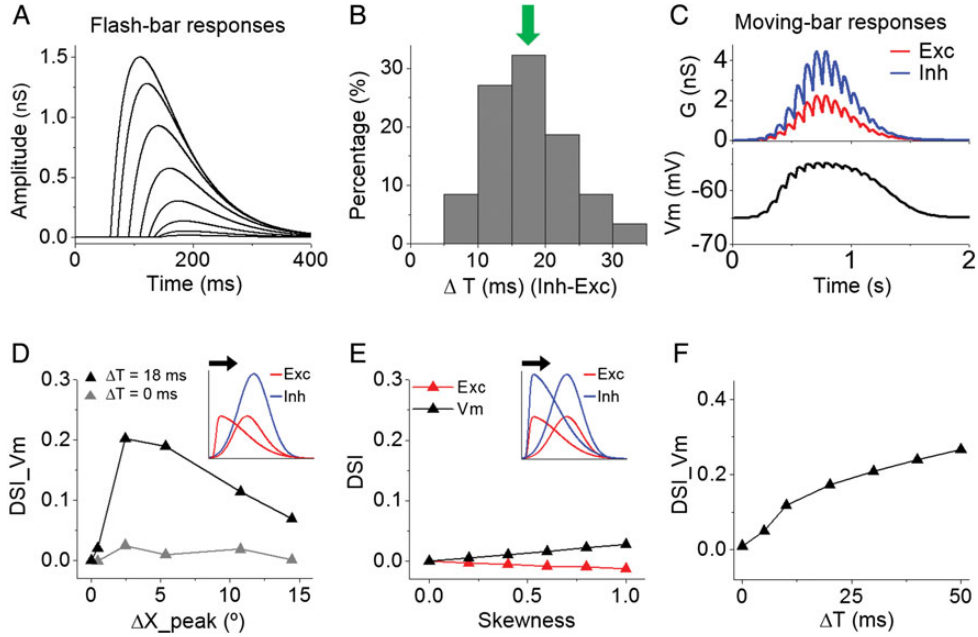

Figure 6. Spatiotemporal offsets between excitation and inhibition contribute to DS. (*A*) Temporal profiles of simulated individual flashing-bar-evoked excitatory responses. The onset latency of each response is negatively correlated with its amplitude (see Materials and Methods). Note that the absolute amplitudes are not important. (*B*) Distribution of onset latency differences between excitation and inhibition evoked by flash stimuli. Arrow points to the mean value (18 ms). The relative delay of inhibition is consistent with previous observations (Liu et al. 2010; Ma et al. 2013) and reflects the disynaptic/polysynaptic nature of inhibition. (*C*) Top, excitatory and inhibitory synaptic conductances in response to a drifting bar, generated by the summation of individual flash-bar-evoked responses. Bottom, membrane potential response derived by integrating the above synaptic conductances in the neuron model. (*D*) DSI of derived membrane potential response plotted against the spatial offset between excitatory and inhibitory RF peaks. The delay of flash-bar-evoked inhibition relative to the excitation was set at 18 (black) or 0 ms (gray). Inset, schematic illustration of varying the skewness of excitatory RF (red curve) while keeping the inhibitory RF (blue curve) symmetric. Black arrow indicates the preferred direction of the cell. (*E*) DSI of excitatory and Vm responses plotted against the skewness of synaptic RFs. Inset, illustration of co-varying the skewness of excitatory and inhibitory RFs. (*F*) DSI of derived membrane potential response as a function of latency of flash-bar-evoked inhibition relative to excitation.

The generation of direction-tuned output response by the spatial offset between excitatory and inhibitory RFs depended on the temporal relationship between flashing-bar-evoked excitatory and inhibitory responses. When the flash-bar-evoked inhibitory response had the same onset delay as the excitatory response (i.e., $\Delta T = 0$ ms), direction-tuned output responses failed to be generated at an optimal spatial offset (Fig. 6*D*, gray). We systematically varied ΔT under a fixed spatial relationship between excitatory and inhibitory RFs. We found that only when the flash-bar-evoked inhibition was delayed relative to excitation (i.e., $\Delta T > 0$ ms), were correctly tuned output responses generated (Fig. 6*F*). Therefore, the contribution of the excitation/inhibition spatial offset to DS relies on an appropriate temporal delay of stationary-stimulus-evoked inhibition relative to excitation.

Discussion

In cats and monkeys, cortical DS appears to be generated *de novo*, because few, if any, thalamic relay cells are found to be direction selective (Wiesel and Hubel 1966; Cleland and Levick 1974; Dreher et al. 1976). Simple cells in the cortical input layer are the first stage where DS is created, and direction-selective simple cells then provide tuned input to direction-selective complex cells (Priebe et al. 2010). The selectivity of simple cells can be attributed to a progressive change of time course of excitatory responses across the RF, which would show a slant when plotted in space and time coordinates (Reid et al. 1987, 1991; DeAngelis et al. 1993; Jagadeesh et al. 1993, 1997). An inhibitory mechanism for DS on the other hand had been more controversial. Very early studies in cats showed that pharmacologically blocking cortical inhibition resulted in a reduction of DS in simple cells (Sillito 1975; Nelson et al. 1994). However, this has now been shown to be an indirect effect of changes in the cell's excitability (Katzner et al. 2011). More recent intracellular recordings have revealed that both excitation and inhibition to simple cells are well tuned for the same direction, attributable to the slanted spatiotemporal organization of inputs (Priebe and Ferster 2005). In addition, because excitation and inhibition are separated in space, they are temporally out of synchrony under moving stimuli of preferred orientation, resulting in a push–pull relationship between excitation and inhibition (Hirsch and Martinez 2006). As such, the temporal separation between excitation and inhibition determines that inhibition does not contribute to sharpening of response selectivity (Priebe and Ferster 2005, 2008).

In the mouse, previous studies suggest that the mechanisms for cortical DS could potentially be different from that in the cat. For example, a small subset of LGN neurons (~10%) are already direction selective (Marshel et al. 2012). While it remains to be determined where these direction-selective LGN neurons project to, they are in principle capable of directly providing direction-tuned excitatory input into the cortex (Piscopo et al. 2013). This notion seems to be supported by a developmental study showing that direction-selective cortical neurons in the mouse V1 already exist right after eye opening and that there are remarkable functional similarities between the development of DS in cortical neurons and that in the mouse retina (Rochefort et al. 2011). More importantly, intracellular recording studies have suggested that there is a large spatial overlap between excitation and inhibition to mouse V1 neurons even for simple cells (Liu et al. 2010, 2011; Tan et al. 2011). As a consequence, under moving stimuli, it is possible to evoke inhibition that is temporally overlapping with excitation, allowing inhibition to contribute to response selectivity by differentially suppressing excitation.

In this study, we directly examined excitatory and inhibitory inputs underlying the DS of layer 4 simple cells in the mouse V1. Similar as observed in the cat (Priebe and Ferster 2005), we found that excitatory inputs are direction-tuned and the preferred direction of excitatory input is the same as that of membrane potential response, indicating that excitatory input provides the seed for DS. However, different from cat simple cells, the tuning of excitatory input cannot be attributed to a unidirectional shift of input latencies across different RF locations, as the latencies are organized into 2 slopes within the synaptic RF (Fig. 5*J*). Our modeling results further demonstrate that a linear summation of excitatory inputs with the observed spatiotemporal organization fails to produce correct direction tuning under moving stimuli (Fig. 6*E*), suggesting that nonlinear mechanisms at thalamocortical synapses or upstream stages are responsible for the tuning of excitatory input. Although tuned, the excitatory input only exhibits moderate selectivity. Due to the nonlinear filtering properties, in particular a saturating input-output transfer function, of the cell membrane (Liu et al. 2011), the excitatory input alone would result in even more weakly tuned membrane potential response (Fig. 4*C*). Fortunately, due to the spatial overlap between excitation and inhibition, moving stimuli evoke inhibition that also overlaps with excitation in the temporal domain. The close temporal interaction of inhibition with excitation leads to a sharpening of DS of membrane potential responses, allowing the selectivity in excitatory inputs to be fully expressed in membrane potential responses (Fig. 4*C*). Eventually, spike threshold further exerts a strong sharpening effect, leading to sharply tuned output responses (Fig. 2*B*). Our finding of inhibitory sharpening of DS is consistent with a recent study showing that reducing visually evoked inhibition by only 10% via optogenetic inactivation of PV inhibitory neurons results in a moderate but significant decrease in DS of cortical responses (Atallah et al. 2012).

Two specific mechanisms contribute to the inhibitory sharpening of DS of output responses. First, excitation is direction-tuned whereas inhibition is largely untuned, resulting in relatively stronger inhibition under null directional movements compared with preferred directional movements. The relatively untuned inhibition is attributable to unselective output responses of inhibitory neurons (Fig. 1*B*). Second, while excitatory and inhibitory RFs are spatially overlapping, the excitatory RF is skewed toward the preferred side of the cell whereas the inhibitory RF is more or less spatially symmetric. These differential spatial distributions of excitatory and inhibitory inputs are translated into differential temporal offsets between peak excitatory and inhibitory responses evoked by moving stimuli of opposite directions: the peak excitation precedes the peak inhibition under preferred directional movements, whereas it is more delayed than the latter under null directional movements. Such specific temporal relationships between excitation and inhibition facilitate a more effective inhibitory suppression of the membrane potential response to the null direction than the preferred and are reminiscent of previous studies in somatosensory and auditory cortices showing that the temporal overlap between excitation and inhibition is different for opposite directional stimuli (Zhang

et al. 2003; Wilent and Contreras 2005). Interestingly, our modeling results demonstrate that a skewed distribution of excitatory inputs plus symmetric distribution of inhibitory inputs is sufficient to result in direction-tuned membrane potential responses even if none of the synaptic responses *per se* is tuned (Fig. 6*D*), providing that stationary-stimulus-evoked inhibition is temporally delayed relative to excitation. These results indicate that the differential spatial tuning of excitation and inhibition is an important factor contributing to the inhibitory sharpening of DS.

Together, our data suggest that the synaptic mechanisms for DS in mouse simple cells are distinct from simple cells in carnivores in several respects. DS of cat simple cells originates from a unidirectional shift of response latencies across the RF, whereas DS of mouse simple cells likely originates from direction-tuned responses in the retina. Excitation and inhibition are organized in a push–pull pattern in cat simple cells, whereas they overlap both spatially and temporally in mouse simple cells. Inhibition does not contribute to DS in cat simple cells, whereas it contributes importantly to sharpening of DS in mouse simple cells. These differences may reflect divergent evolutionary solutions to generating DS in visual cortex. The observed spatial and temporal overlap of excitation and inhibition in mouse simple cells resonates with recent theoretical models of cortical signal processing where excitatory and inhibitory inputs are dynamically correlated (Vogels and Abbott 2009; Kremkow et al. 2010).

Our study also raises several interesting questions to be investigated in the future. For example, how do skewed excitatory RFs arise while inhibitory RFs are all symmetric? Previous experimental and modeling studies have demonstrated that repeated directional stimuli can induce an asymmetric shaping of cortical synaptic circuits through spike-timing-dependent plasticity (STDP) (Mehta et al. 2000; Rao and Sejnowski 2000; Engert et al. 2002; Fu et al. 2004; Wenisch et al. 2005). These results suggest that asymmetric RFs may arise through activity-dependent mechanisms. Since the development of DS in mouse V1 neurons is not affected by rearing animals in darkness (Rochefort et al. 2011), it is possible that some endogenously generated activity waves are sufficient to drive the formation of asymmetric excitatory RFs. Likely, some directional bias provided by retinal/thalamic input exists to facilitate symmetry-breaking under activity waves of all different directions (Li et al. 2008), which may explain why the excitatory RF is always skewed toward the preferred side and why not all excitatory cells have asymmetric RFs. Noticeably, the STDP-dependent asymmetric modification of synaptic circuits only applies to excitatory connections, whereas the activity-dependent plasticity of inhibitory connections or that of excitatory synapses onto inhibitory neurons is not sensitive to the temporal order of pre- and post-synaptic spiking (Bi and Poo 2001; Woodin et al. 2003; Lu et al. 2007). This may explain why asymmetric inhibitory RFs do not develop. Finally, the nonselective property of inhibitory neurons well explains the untuned inhibitory input, but also raises the question of why they are different from excitatory neurons. Do these neurons all receive untuned excitatory inputs, or do their inhibitory inputs display properties that prevent them from effectively suppressing the null response? Future intracellular recordings from inhibitory neurons are required to address this question.

Funding

This work was supported by the National Eye Institute at the National Institutes of Health (RO1 EY019049 and R21 EY022478 to H.W.T.) and the Kirchgessner Foundation. L.I.Z. was supported by the National Institute of Health (RO1DC008983) and the David and Lucile Packard Foundation.

Notes

Conflict of Interest: None declared.

References

Adelson EH, Bergen JR. 1985. Spatiotemporal energy models for the perception of motion. J Opt Soc Am A. 2:284–299.

Albrecht DG, Geisler WS. 1991. Motion selectivity and the contrast-response function of simple cells in the visual cortex. Vis Neurosci. 7:531–546.

Atallah BV, Bruns W, Carandini M, Scanziani M. 2012. Parvalbumin-expressing interneurons linearly transform cortical responses to visual stimuli. Neuron. 73:159–170.

Barlow HB, Levick WR. 1965. The mechanism of directionally selective units in rabbit's retina. J Physiol. 178:477–504.

Bi G, Poo M. 2001. Synaptic modification by correlated activity: Hebb's postulate revisited. Annu Rev Neurosci. 24:139–166.

Cleland BG, Levick WR. 1974. Properties of rarely encountered types of ganglion cells in the cat's retina and an overall classification. J Physiol. 240:457–492.

Conway BR, Livingstone MS. 2003. Space-time maps and two-bar interactions of different classes of direction-selective cells in macaque V-1. J Neurophysiol. 89:2726–2742.

DeAngelis GC, Ohzawa I, Freeman RD. 1993. Spatiotemporal organization of simple-cell receptive fields in the cat's striate cortex. II. Linearity of temporal and spatial summation. J Neurophysiol. 69:1118–1135.

Dreher B, Fukada Y, Rodieck RW. 1976. Identification, classification and anatomical segregation of cells with X-like and Y-like properties in the lateral geniculate nucleus of old-world primates. J Physiol. 258:433–452.

Emerson RC. 1997. Quadrature subunits in directionally selective simple cells: spatiotemporal interactions. Vis Neurosci. 14:357–371.

Engert F, Tao HW, Zhang LI, Poo MM. 2002. Moving visual stimuli rapidly induce direction sensitivity of developing tectal neurons. Nature. 419:470–475.

Fu YX, Shen Y, Gao H, Dan Y. 2004. Asymmetry in visual cortical circuits underlying motion-induced perceptual mislocalization. J Neurosci. 24:2165–2171.

Hesam Shariati N, Freeman AW. 2012. A multi-stage model for fundamental functional properties in primary visual cortex. PLoS One. 7: e34466.

Hirsch JA, Martinez LM. 2006. Circuits that build visual cortical receptive fields. Trends Neurosci. 29:30–39.

Hubel DH, Wiesel TN. 1962. Receptive fields, binocular interaction and functional architecture in the cat's visual cortex. J Physiol. 160: 106–154.

Jagadeesh B, Wheat HS, Ferster D. 1993. Linearity of summation of synaptic potentials underlying direction selectivity in simple cells of the cat visual cortex. Science. 262:1901–1904.

Jagadeesh B, Wheat HS, Kontsevich LL, Tyler CW, Ferster D. 1997. Direction selectivity of synaptic potentials in simple cells of the cat visual cortex. J Neurophysiol. 78:2772–2789.

Jin J, Wang Y, Lashgari R, Swadlow HA, Alonso JM. 2011. Faster thalamocortical processing for dark than light visual targets. J Neurosci. 31:17471–17479.

Katzner S, Busse L, Carandini M. 2011. GABAA Inhibition Controls Response Gain in Visual Cortex. J Neurosci. 31:5931–5941.

Kremkow J, Aertsen A, Kumar A. 2010. Gating of signal propagation in spiking neural networks by balanced and correlated excitation and inhibition. J Neurosci. 30:15760–15768.
Li LY, Li YT, Zhou M, Tao HW, Zhang LI. 2013. Intracortical multiplication of thalamocortical signals in mouse auditory cortex. Nat Neurosci. 16:1179–1181.
Li Y, Van Hooser SD, Mazurek M, White LE, Fitzpatrick D. 2008. Experience with moving visual stimuli drives the early development of cortical direction selectivity. Nature. 456:952–956.
Li YT, Ibrahim LA, Liu BH, Zhang LI, Tao HW. 2013. Linear transformation of thalamocortical input by intracortical excitation. Nat Neurosci. 16:1324–1330.
Li YT, Ma WP, Li LY, Ibrahim LA, Wang SZ, Tao HW. 2012. Broadening of inhibitory tuning underlies contrast-dependent sharpening of orientation selectivity in mouse visual cortex. J Neurosci. 32: 16466–16477.
Li YT, Ma WP, Pan CJ, Zhang LI, Tao HW. 2012. Broadening of cortical inhibition mediates developmental sharpening of orientation selectivity. J Neurosci. 32:3981–3991.
Lien AD, Scanziani M. 2013. Tuned thalamic excitation is amplified by visual cortical circuits. Nat Neurosci. 16:1315–1323.
Liu BH, Li P, Li YT, Sun YJ, Yanagawa Y, Obata K, Zhang LI, Tao HW. 2009. Visual receptive field structure of cortical inhibitory neurons revealed by two-photon imaging guided recording. J Neurosci. 29:10520–10532.
Liu BH, Li YT, Ma WP, Pan CJ, Zhang LI, Tao HW. 2011. Broad inhibition sharpens orientation selectivity by expanding input dynamic range in mouse simple cells. Neuron. 71:542–554.
Liu BH, Li P, Sun YJ, Li YT, Zhang LI, Tao HW. 2010. Intervening inhibition underlies simple-cell receptive field structure in visual cortex. Nat Neurosci. 13:89–96.
Livingstone MS. 1998. Mechanisms of direction selectivity in macaque V1. Neuron. 20:509–526.
Lu JT, Li CY, Zhao JP, Poo MM, Zhang XH. 2007. Spike-timing-dependent plasticity of neocortical excitatory synapses on inhibitory interneurons depends on target cell type. J Neurosci. 27: 9711–9720.
Ma WP, Li YT, Tao HW. 2013. Downregulation of cortical inhibition mediates ocular dominance plasticity during the critical period. J Neurosci. 33:11276–11280.
Ma WP, Liu BH, Li YT, Huang ZJ, Zhang LI, Tao HW. 2010. Visual representations by cortical somatostatin inhibitory neurons—selective but with weak and delayed responses. J Neurosci. 30:14371–14379.
Mangini NJ, Pearlman AL. 1980. Laminar distribution of receptive field properties in the primary visual cortex of the mouse. J Comp Neurol. 193:203–222.
Marshel JH, Kaye AP, Nauhaus I, Callaway EM. 2012. Anterior-posterior direction opponency in the superficial mouse lateral geniculate nucleus. Neuron. 76:713–720.
McLean J, Palmer LA. 1989. Contribution of linear spatiotemporal receptive field structure to velocity selectivity of simple cells in area 17 of cat. Vision Res. 29:675–679.
Mehta MR, Quirk MC, Wilson MA. 2000. Experience-dependent asymmetric shape of hippocampal receptive fields. Neuron. 25: 707–715.
Monier C, Chavane F, Baudot P, Graham LJ, Fregnac Y. 2003. Orientation and direction selectivity of synaptic inputs in visual cortical neurons: a diversity of combinations produces spike tuning. Neuron. 37:663–680.
Moore CI, Nelson SB. 1998. Spatio-temporal subthreshold receptive fields in the vibrissa representation of rat primary somatosensory cortex. J Neurophysiol. 80:2882–2892.
Movshon JA, Thompson ID, Tolhurst DJ. 1978. Spatial and temporal contrast sensitivity of neurones in areas 17 and 18 of the cat's visual cortex. J Physiol. 283:101–120.
Nelson S, Toth L, Sheth B, Sur M. 1994. Orientation selectivity of cortical neurons during intracellular blockade of inhibition. Science. 265:774–777.
Niell CM, Stryker MP. 2008. Highly selective receptive fields in mouse visual cortex. J Neurosci. 28:7520–7536.
Piscopo DM, El-Danaf RN, Huberman AD, Niell CM. 2013. Diverse visual features encoded in mouse lateral geniculate nucleus. J Neurosci. 33:4642–4656.
Priebe NJ, Ferster D. 2005. Direction selectivity of excitation and inhibition in simple cells of the cat primary visual cortex. Neuron. 45:133–145.
Priebe NJ, Ferster D. 2008. Inhibition, spike threshold, and stimulus selectivity in primary visual cortex. Neuron. 57:482–497.
Priebe NJ, Lampl I, Ferster D. 2010. Mechanisms of direction selectivity in cat primary visual cortex as revealed by visual adaptation. J Neurophysiol. 104:2615–2623.
Rao RPN, Sejnowski TJ. 2000. Predictive sequence learning in recurrent neocortical circuits. In: SA S, TK L, KR M, editors. Advances in neural information processing systems. Cambridge, MA: MIT.
Reid RC, Soodak RE, Shapley RM. 1991. Directional selectivity and spatiotemporal structure of receptive fields of simple cells in cat striate cortex. J Neurophysiol. 66:505–529.
Reid RC, Soodak RE, Shapley RM. 1987. Linear mechanisms of directional selectivity in simple cells of cat striate cortex. Proc Natl Acad Sci USA. 84:8740–8744.
Rochefort NL, Narushima M, Grienberger C, Marandi N, Hill DN, Konnerth A. 2011. Development of direction selectivity in mouse cortical neurons. Neuron. 71:425–432.
Schiller PH, Finlay BL, Volman SF. 1976. Quantitative studies of single-cell properties in monkey striate cortex. II. Orientation specificity and ocular dominance. J Neurophysiol. 39:1320–1333.
Scholl B, Tan AY, Corey J, Priebe NJ. 2013. Emergence of orientation selectivity in the Mammalian visual pathway. J Neurosci. 33: 10616–10624.
Sillito AM. 1975. The contribution of inhibitory mechanisms to the receptive field properties of neurones in the striate cortex of the cat. J Physiol. 250:305–329.
Skottun BC, De Valois RL, Grosof DH, Movshon JA, Albrecht DG, Bonds AB. 1991. Classifying simple and complex cells on the basis of response modulation. Vision Res. 31:1079–1086.
Tan AY, Brown BD, Scholl B, Mohanty D, Priebe NJ. 2011. Orientation selectivity of synaptic input to neurons in mouse and cat primary visual cortex. J Neurosci. 31:12339–12350.
Torre V, Poggio T. 1978. A synaptic mechanism possibly underlying directional selectivity to motion. Proc R Soc Lond Ser B. 202:409–416.
Vogels TP, Abbott L. 2009. Gating multiple signals through detailed balance of excitation and inhibition in spiking networks. Nature Neurosci. 12:483–491.
Wenisch OG, Noll J, Hemmen JL. 2005. Spontaneously emerging direction selectivity maps in visual cortex through STDP. Biol Cybern. 93:239–247.
Wiesel TN, Hubel DH. 1966. Spatial and chromatic interactions in the lateral geniculate body of the rhesus monkey. J Neurophysiol. 29: 1115–1156.
Wilent WB, Contreras D. 2005. Dynamics of excitation and inhibition underlying stimulus selectivity in rat somatosensory cortex. Nat Neurosci. 8:1364–1370.
Woodin MA, Ganguly K, Poo MM. 2003. Coincident pre- and postsynaptic activity modifies GABAergic synapses by postsynaptic changes in Cl-transporter activity. Neuron. 39:807–820.
Wu GK, Arbuckle R, Liu BH, Tao HW, Zhang LI. 2008. Lateral sharpening of cortical frequency tuning by approximately balanced inhibition. Neuron. 58:132–143.
Zhang LI, Tan AY, Schreiner CE, Merzenich MM. 2003. Topography and synaptic shaping of direction selectivity in primary auditory cortex. Nature. 424:201–205.
Zhang M, Liu Y, Wang SZ, Zhong W, Liu BH, Tao HW. 2011. Functional elimination of excitatory feedforward inputs underlies developmental refinement of visual receptive fields in zebrafish. J Neurosci. 31:5460–5469.
Zhao X, Chen H, Liu X, Cang J. 2013. Orientation-selective responses in the mouse lateral geniculate nucleus. J Neurosci. 33:12751–12763.
Zhou Y, Liu BH, Wu GK, Kim YJ, Xiao Z, Tao HW, Zhang LI. 2010. Preceding inhibition silences layer 6 neurons in auditory cortex. Neuron. 65:706–717.